This is an open access article published under an ACS AuthorChoice License, which permits copying and redistribution of the article or any adaptations for non-commercial purposes.

ACS AUTHORCHOICE

THE JOURNAL OF PHYSICAL CHEMISTRY C

Article

Cite This: J. Phys. Chem. C 2019, 123, 28255−28265

pubs.acs.org/JPCC

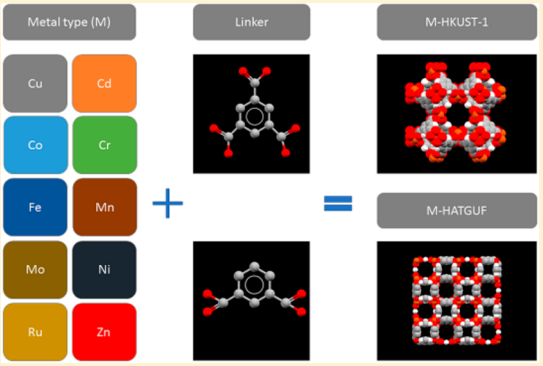
In Silico Design of Metal Organic Frameworks with Enhanced CO_2 Separation Performances: Role of Metal Sites

Gokay Avci, Sadiye Velioglu, and Seda Keskin*

Department of Chemical and Biological Engineering, Koc University, Rumelifeneri Yolu, Sariyer 34450, Istanbul, Turkey

Supporting Information

ABSTRACT: In this study, grand canonical Monte Carlo simulations were performed to investigate the impact of metal centers on CO_2/H_2 mixture adsorption and separation performance of two different metal organic framework (MOF) series, M-HKUST-1 and M-HATGUF, where M represents different metals: Cd, Co, Cr, Cu, Fe, Mn, Mo, Ni, Ru, and Zn. Results show that the type of metal site affects the CO_2 and H_2 uptakes of MOFs, and as a result, adsorbent performance metrics of MOFs such as selectivity, working capacity, regenerability, and adsorbent performance score significantly vary depending on the metal type. Cr-HKUST-1 and Cd-HKUST-1 were identified to have 11% and 38% enhanced CO_2/H_2 selectivities in addition to 27% and 60% enhanced adsorbent performance scores compared to original Cu-HKUST-1, respectively. CO_2/H_2 selectivity of HATGUF was found to be almost doubled by changing the metal from Cu to Cd in addition to 142% increase in the adsorbent performance score of HATGUF. Our results revealed that changing the metal type of MOFs offers a great opportunity in the way of improving the CO_2/H_2 separation performance of materials. Considering the very large number of available MOFs and metals, these results will be useful to design new MOFs by directing the selection of metals that will lead to high-performance adsorbents for CO_2 capture.



1. INTRODUCTION

Metal organic frameworks (MOFs) have been recently considered as highly promising adsorbents for CO_2 capture due to their high adsorption capacities and versatilities in their chemical structures.[1−3] MOFs have unique properties such as high porosities and large surface areas in addition to their wide range of pore sizes and shapes which make them potentially promising adsorbent materials for CO_2 separation from different gases.[3,4] Several experimental and computational studies showed that MOFs can outperform many zeolite adsorbents in CO_2 capture[5−8] and CO_2/H_2 separation.[9−12] A new route in enhancing the CO_2 separation potential of MOFs, which are composed of metal centers connected by organic linkers, is the metal substitution. Different methods such as reticular design,[13] metal doping,[14] and cluster metalation through stepwise synthesis[15] were proposed to synthesize MOF materials with metal substitution which lead to M-MOF series where M corresponds to the metal. The impact of using different metal types on the CO_2, CH_4, and H_2O adsorption properties of MOFs has been reported for some materials such as HKUST-1, CPO-27, MOF-74, and UiO-66.[16−19] Synthesis of M-MOF series by maintaining permanent porosity and original crystallographic symmetry of the structure is challenging. Furthermore, due to the large number of available metals, it is not straightforward to experimentally synthesize MOFs using every single metal and test all these MOFs for a target gas adsorption and/or separation process. Computational studies have been recently used to alter the metal type of MOFs to uncover the effect of metal type on the CO_2 capture and separation performance of MOFs.

HKUST-1 is one of the most widely studied MOFs in computational studies due to its high gas adsorption capacity.[8,20] Wu et al.[21] computationally investigated adsorption properties of methanol and acetone in M-HKUST-1 and found that adsorption capacities of MOFs generally follow the order of Ti > Fe > Cu > Co > Mo > Ru-HKUST-1. They discussed that adsorption performance of the MOF was dictated by the adsorbate−framework interactions at low pressures whereas structural properties such as pore volume and accessible surface area are the predominant factors for gas adsorption at high pressures. Yu et al.[22] computationally focused on four different M-HKUST-1 materials (M = Zn, Co, Ni, and Mg) and found that hydrated Co-, Ni-, and Zn-HKUST-1 showed improved CO_2 adsorption compared to their nonhydrated counterparts. Coulombic interactions between CO_2 molecules and the electric field created by the coordinated water molecules were found to be responsible for the increased CO_2 uptake in these MOFs. Koh et al.[23] used density functional theory (DFT) calculations and modified the UFF (universal force field) parameters to better fit CH_4

Received: September 9, 2019
Revised: October 28, 2019
Published: October 29, 2019

Downloaded via 85.98.159.57 on March 31, 2020 at 08:51:56 (UTC).
See https://pubs.acs.org/sharingguidelines for options on how to legitimately share published articles.

© 2019 American Chemical Society

DOI: 10.1021/acs.jpcc.9b08581
J. Phys. Chem. C 2019, 123, 28255−28265

adsorption in M-HKUST-1 where 17 different metals were investigated. They showed that CH_4 adsorption increases with increasing metal point charge. In addition to HKUST-1, IRMOF-10 and MOF-74 series have been also studied to understand the role of metal type in gas adsorption capacities of MOFs. Borycz et al.[24] developed a force field to investigate the CO_2 adsorption in M-IRMOF-10 series where M corresponds to Mg, Ca, Fe, Cu, Zn, Ge, Sr, Cd, Sn, and Ba. They reported that CO_2 adsorption of Ba-IRMOF-10 at low pressure was almost doubled compared to that of Zn-IRMOF-10 due to the larger ionic radii of Ba which was exposed more to CO_2 by reducing the steric hindrance.[24] Park et al.[25] performed the DFT calculations and showed that M-MOF-74 can be tuned in order to have a stronger binding affinity for CO_2 by metal substitution with Ti, and V. Canepa et al.[26] examined the binding characteristics of single-component gases such as H_2, CO_2, CH_4, and H_2O in M-MOF-74 series having 25 different metal types using the DFT calculations and reported that CO_2 interactions were higher with Rh, Pd, Os, Ir, and Pt metals compared to the rest of the metals.

It has been discussed in the literature that dominant factors affecting the adsorption of single-component gases were charge environment of the framework at low-pressure regime, heat of adsorption of the gas at medium pressures, and geometrical factors of MOFs such as surface area and porosity at higher pressures.[27−29] Effects of these factors become more complex when adsorption of a gas mixture is considered due to the competitive and/or cooperative adsorption of different species in MOFs. Both computational and experimental studies have shown that single-component gas adsorption can be tuned by the change of metal type as briefly summarized above. On the other hand, there has been a very limited number of studies investigating the impact of metal type on the gas mixture separation performance of MOFs. Poor et al.[30] examined M-HKUST-1 (M = Mn, Fe, Co, Ni, and Zn) for anesthetic gas separation and proposed that Ni-HKUST-1 can improve the uptake and selectivity of Xe with respect to CO_2. Sholl and co-workers[31] investigated M-HKUST-1 and showed that material with Zn atom has the highest C_2H_2/C_2H_6 selectivity where impurities can also be sequentially filtered by the use of MOFs having metals such as Ru, Ti, and Ni.[31]

As this literature review shows, almost all computational studies have focused on the impact of the metal type on the single-component gas uptake or selectivity of some common MOFs. Although selectivity is an important criterion in selection of the adsorbent materials, several other adsorbent performance metrics such as working capacity, regenerability, and adsorbent performance score are equally important in choosing materials for separation of gas mixtures. Motivated from these, we specifically investigated the role of metal type on the adsorption-based CO_2/H_2 separation performances of two MOFs using molecular simulations. First, we focused on the widely studied HKUST-1 since metal substitution was experimentally used to successfully synthesize some types of M-HKUST-1 materials without sacrificing the original crystallographic information. The second MOF we examined is HATGUF since it was identified as one of the best adsorbent candidates for CO_2/H_2 separation in our previous high-throughput computational screening study[9] where adsorption-based separation performances of 3857 different MOFs were investigated. The Cu metal of these two MOFs was changed with nine different metals, Cd, Co, Cr, Fe, Mn, Mo, Ni, Ru, and Zn, to examine the effect of metal type on the CO_2/H_2 mixture separation performance of M-HKUST-1 and M-HATGUF series using grand canonical Monte Carlo (GCMC) simulations. Various adsorbent performance metrics including adsorption selectivity, working capacity, adsorbent performance score, and regenerability were computed at both pressure swing adsorption (PSA) and vacuum swing adsorption (VSA) conditions for each MOF to assess which metal type has the best improvement on these metrics of M-HKUST-1 and M-HATGUF materials. Molecular-level insights obtained from this study will be useful in guiding the metal substitution of the existing MOFs that can lead to adsorbents with enhanced CO_2/H_2 separation performances in addition to directing the metal selection during the MOF synthesis studies to achieve better gas adsorption and separation performances.

2. COMPUTATIONAL DETAILS

2.1. MOFs. HKUST-1 (refcode: FIQCEN) is one of the most widely studied MOFs in the literature due to its structural properties and ability to be synthesized using different methods with a high purity and yield. Its largest cavity diameter (LCD) and pore limiting diameter (PLD) were calculated as 13.2 and 6.65 Å, respectively, by Zeo++ software,[32] and it has an intersecting three-dimensional channel framework. HATGUF, which was identified as one of the top performing MOFs for CO_2/H_2 separation in our recent work,[9] was also examined in this work since HATGUF has a comparable chemical structure with HKUST-1: (i) HATGUF has the same metal, Cu, with HKUST-1. (ii) HATGUF has benzene dicarboxylate linker instead of benzene tricarboxylate; thus, it has a different linker−node connection leading to different topology where each linker is connected to two paddle wheel nodes instead of three different nodes in HKUST-1. (iii) The PLD of HATGUF, 6.67 Å, was calculated to be similar to that of HKUST-1, 6.65 Å, but HATGUF has a comparably smaller LCD, 8.42 Å. (iv) Similar to the HKUST-1, removal of coordinated solvent molecules in HATGUF led to coordinately unsaturated metal sites. Structural representations of these two MOFs showing their distinct pores are given in Figure S1 of the Supporting Information.

In order to investigate the effect of metal type on the CO_2/H_2 separation performance of HKUST-1 and HATGUF, we studied 10 different metals: Cd, Co, Cr, Cu, Fe, Mn, Mo, Ni, Ru, and Zn. Cu was the original metal of these two MOFs, and the other metals were selected to study the transition metals. Prior to metal change, bound and unbound solvent molecules of both HKUST-1 and HATGUF structures were manually cleaned. Metal change and optimization of MOF structures were carried out using the Material Studio 2017 R2.[33] Structures were modified by replacing the metal center, Cu atoms, with the other metals using the tool "modify element" in the Material Studio. Energy minimization with a convergence tolerance quality of fine (energy tolerance value of 10^{-4} kcal/mol) and geometry optimization using the Smart algorithm with maximum iteration numbers of 1000 were performed for both M-HKUST-1 and M-HATGUF series using the Forcite module. The convergence tolerances in geometry optimization were set as 10^{-6} Å, 10^{-5} kcal/mol, and 10^{-4} kcal/mol × Å for the displacement, energy, and force, respectively. During this step, the cell parameters of the frameworks were allowed to be relaxed as well. Optimization of M-MOF series was conducted by using the potential parameters taken from the UFF.[34] Partial charge assignment to framework atoms was performed using Qeq (charge

DOI: 10.1021/acs.jpcc.9b08581
J. Phys. Chem. C 2019, 123, 28255−28265

Table 1. Nonbonded Interaction Parameters of Metals and Structural Properties of M-HKUST-1 and M-HATGUF Materials

MOF	ε_{metal}/k_B (K)	σ_{metal} (Å)	q_{metal} (e^-)	PLD (Å)	LCD (Å)	surface area (m^2/g)	pore volume (cm^3/g)
Cd-HKUST-1	114.8	2.54	1.21	6.72	13.44	1870.8	0.70
Co-HKUST-1	7.04	2.56	1.00	6.34	12.02	2095.5	0.77
Cr-HKUST-1	7.55	2.69	1.13	6.47	12.15	2292.7	0.83
Cu-HKUST-1	3.11	2.51	0.99	6.65	13.19	2159.7	0.82
Fe-HKUST-1	6.54	2.59	0.85	6.49	12.20	2248.9	0.82
Mn-HKUST-1	6.54	2.63	0.97	6.53	12.24	2309.4	0.84
Mo-HKUST-1	28.19	2.71	1.12	6.71	12.36	2032.4	0.73
Ni-HKUST-1	7.55	2.52	1.12	6.22	12.60	1898.3	0.75
Ru-HKUST-1	28.19	2.64	1.03	6.74	12.41	2015.4	0.72
Zn-HKUST-1	62.44	2.46	1.19	6.29	13.29	1861.0	0.75
Cd-HATGUF	114.8	2.54	1.21	7.36	8.78	913.2	0.46
Co-HATGUF	7.04	2.56	1.01	6.55	7.31	926.3	0.47
Cr-HATGUF	7.55	2.69	1.15	6.95	7.71	1054.0	0.53
Cu-HATGUF	3.11	2.51	0.99	6.67	8.42	918.1	0.50
Fe-HATGUF	6.54	2.59	0.84	6.96	7.68	1041.8	0.52
Mn-HATGUF	6.54	2.63	0.96	7.01	7.71	1056.9	0.53
Mo-HATGUF	28.19	2.71	1.09	7.31	8.22	931.1	0.48
Ni-HATGUF	7.55	2.52	1.15	6.27	7.22	878.8	0.46
Ru-HATGUF	28.19	2.64	0.99	7.36	8.35	921.0	0.47
Zn-HATGUF	62.44	2.46	1.21	6.22	7.21	824.9	0.43

equilibration method)[35] and EQeq (extended charge equilibration method)[36] methods depending on the existing metal type in order to compute the electrostatic interactions between MOF atoms and gas molecules. Charge assignment method used for the M-MOF materials was chosen to best reproduce the available experimental gas adsorption data as explained in detail in Section 2.2.

Molecular simulation techniques that we described in our previous high-throughput computational screening study[9] were used. Briefly, we used Zeo++ software[32] to calculate structural properties of M-MOF series such as surface area, PLD, LCD, and pore volume which were provided in Table 1. Nitrogen with a probe radius of 1.87 Å and a probe with 0 Å radius were used to calculate surface area and pore volume, respectively, via 2 000 and 50 000 iterations. Lennard-Jones (LJ) parameters and partial charges of metal atoms and structural properties of optimized M-HKUST-1 and M-HATGUF series are all provided in Table 1. It is important to note that structural properties of M-HKUST-1 and M-HATGUF series do not significantly differ from the original HKUST-1 and HATGUF structures, indicating efficient structure optimization using UFF. The PLD and LCD values for M-HKUST-1 (M-HATGUF) series range from 6.22 to 6.74 Å and from 12.02 to 13.44 Å (6.22−7.36 Å and 7.21−8.78 Å), respectively. Surface areas of M-HKUST-1 (M-HATGUF) series were calculated to be in the range of 1861−2309 m^2/g (825−1057 m^2/g) whereas their pore volumes were computed as 0.70−0.84 cm^3/g (0.43−0.53 cm^3/g).

2.2. Molecular Simulation. In order to calculate gas uptakes of optimized M-HKUST-1 and M-HATGUF series, GCMC simulations were carried using the RASPA software.[37] Similar to the optimization step, UFF was used as the force field. Qeq and EQeq methods were used for the charge assignment, and Table S1 shows the partial charges of framework atoms for M-HKUST-1 and M-HATGUF series. Gas−gas and gas−MOF interactions were defined using the LJ potential. Single-site spherical and three-site rigid LJ 12-6 potentials were used to model H_2 and CO_2, respectively.[38,39] The Lorentz−Berthelot mixing rules were employed for pair interactions. For electrostatic interactions, Ewald summation with 10^{-6} precision was used. The cutoff radius was set to 12.5 Å according to the length of the unit cell of M-MOF series, and periodic boundary conditions were applied in all dimensions. Simulations were performed with 5 000 cycles for initialization and 100 000 cycles for production runs. We studied both CO_2/H_2:15/85 and CO_2/H_2:50/50 mixtures at 298 K at three different pressures, 0.1, 1, and 10 bar, to investigate the effect of operating conditions and composition of the mixture on the gas separation performances of MOFs. In order to mimic PSA (VSA) process, adsorption and desorption pressures were set to 10 (1) and 1 (0.1) bar, respectively. Results of molecular simulations were used to compute CO_2/H_2 adsorption selectivity, CO_2 working capacity, percent regenerability (R %), and adsorbent performance score (APS) of MOFs. Table S2 gives the definitions of these metrics. Briefly, adsorption selectivity is the ratio of adsorbed amount of CO_2 to that of H_2 normalized by their bulk compositions; working capacity is the difference in the adsorbed CO_2 amount computed at adsorption and desorption pressures; APS is the multiplication of selectivity and working capacity; and R% represents the gas amount that can be regenerated through PSA or VSA cycles. The values of isosteric heat of adsorption of CO_2 and H_2 were also computed using the fluctuation method[40] to assess the affinity of MOFs to CO_2 and H_2 molecules. We also computed the volume-rendered density plots of adsorbate positions using VTK (The Visualization Toolkit) as implemented in the RASPA. The unit cell of MOF was divided into 150 × 150 × 150 voxels, and positions of adsorbate molecules were mapped into the corresponding voxels during GCMC simulations. The data were then normalized using the highest occurring voxel value from the final data of 100 000 production runs, and the density plots of positions of adsorbed CO_2 and H_2 molecules within the unit cell of M-HKUST-1 and M-HATGUF were generated.

We first compared our molecular simulation results for M-HKUST-1 materials with the available experimental and simulated data in the literature to validate the accuracy of our computational approach. We tried using two different

DOI: 10.1021/acs.jpcc.9b08581
J. Phys. Chem. C 2019, 123, 28255−28265

charge assignment methods, Qeq and EQEq, to identify the method that best reproduces the available experimental and/or computational gas adsorption isotherms. Qeq assumes a neutral oxidation state whereas oxidation states can be defined in the EQeq method. Figure 1a–e compares our simulation

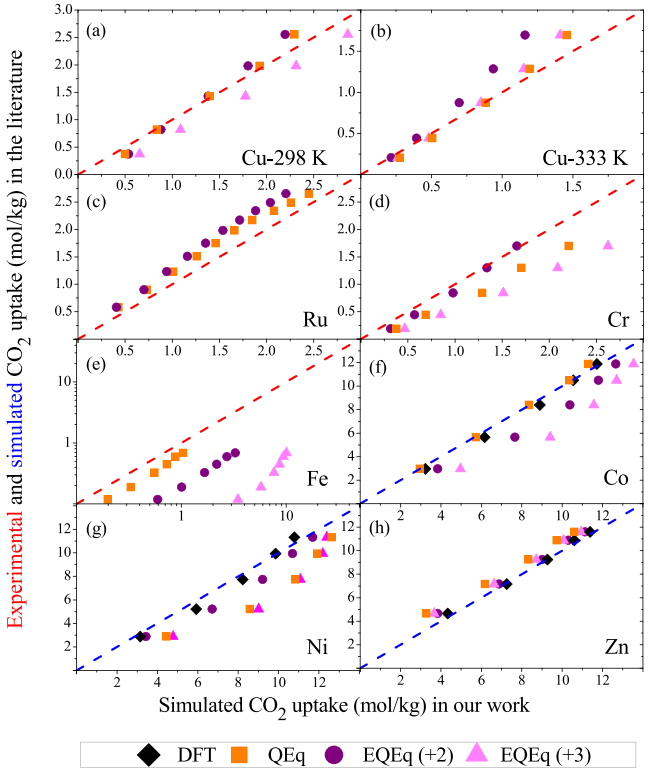


Figure 1. Comparison of our simulated CO_2 uptakes in M-HKUST-1 materials with the available experimental and simulation data at 0.1–1 bar, 298 K unless otherwise stated in the figure. Red and blue dotted diagonal lines represent experimental and simulated data comparison, respectively. Orange, purple, pink, and black data points represent the simulated CO_2 uptakes obtained by using QEq, EQeq method with +2 oxidation state, EQeq method with +3 oxidation state, and DFT charges provided in the literature,[22] respectively.

results with the experimental CO_2 uptakes of Cu-HKUST-1 (at 298 K),[19] Cu-HKUST-1 (at 333 K),[41] Ru-HKUST-1,[42] Cr-HKUST-1,[19] and Fe-HKUST-1[41] under the same conditions. At two different adsorption temperatures, Qeq charges resulted in a good agreement with the experimental adsorption data of Cu-HKUST-1 in the whole pressure range as shown in Figure 1a and b. Similarly, for Ru- and Fe-HKUST-1 as shown in Figure 1c and e, the Qeq method gave a better agreement with the experiments compared to the EQeq method. For Cr-HKUST-1, a very good agreement was observed between the experimental and simulated adsorption isotherm using the partial charges assigned by the EQeq method with +2 oxidization states as shown in Figure 1d. Figure 1f–h compares our simulation results with the previous simulation data of CO_2 uptakes in Co-, Ni-, and Zn-HKUST-1 using the DFT-based charges.[22] The CO_2 uptakes calculated using the DFT-based charges matched well with the ones we calculated using the Qeq method for Co-HKUST-1. For Ni-HKUST-1 and Zn-HKUST-1, we observed a good agreement between the CO_2 adsorption data computed by the DFT charges and the one we computed using the EQeq method with +2 oxidization state. The EQeq method was also used for Cd-HKUST-1 since we observed positive Coulombic energy between gas molecules and MOF atoms when the Qeq method was used. There was no data in the literature for comparison of Mn- and Mo-HKUST-1; therefore, we preferred using the Qeq method. Overall, the EQeq method with +2 oxidization state was used to assign the partial charges of HKUST-1 and HATGUF having Ni, Cr, Cd, and Zn whereas the Qeq method was used for the rest of the metals. Figure 1 shows the simulated CO_2 uptakes of M-HKUST-1 obtained at a pressure range of 0.1–1 bar, and we also presented the CO_2 adsorption isotherms of M-HKUST-1 and M-HATGUF series up to 20 bar in Figure S2.

3. RESULTS AND DISCUSSIONS

The CO_2 and H_2 uptakes of M-HKUST-1 series for CO_2/H_2:15/85 mixture at 0.1, 1, and 10 bar, 298 K are shown in Figure 2. In each figure, metal charges of MOFs, difference of heats of adsorption values between CO_2 and H_2, and surface area of MOFs were color-coded to examine their effects on the CO_2 and H_2 adsorption of adsorbents having different metals. Figure 2a shows that as the value of metal charge increases, CO_2 adsorption increases whereas H_2 adsorption decreases for all MOFs except Mo-, Ru-, and Cd-HKUST-1. The increase in CO_2 uptake can be explained by the increase in the electrostatic interactions between CO_2 molecules and MOF atoms. On the other hand, the decrease in H_2 adsorption can be attributed to the occupation of CO_2 molecules around the favorable adsorption sites in the framework. Three MOFs, Mo-, Ru-, and Cd-HKUST-1, are located at a different region which can be attributed to their large ionic radii that hinder the available free volume around the metal centers for H_2 adsorption. Figure 2b shows that M-HKUST-1 materials having high CO_2 uptakes are the ones having the largest difference between the heat of adsorption values of two gases ($\Delta Q_{st} = Q_{st}^{CO_2} - Q_{st}^{H_2}$). For all MOFs, $Q_{st}^{H_2}$values were calculated to be almost the same, 5.37–5.75 kJ/mol, but $Q_{st}^{CO_2}$ values were computed to vary from 23.9 to 25.5 kJ/mol, indicating that metal type has a more pronounced effect on the CO_2 uptake than H_2 uptake. Figure 2c represents that there is not a direct relation between the gas uptakes and surface areas of MOFs, in agreement with the literature where it was shown that simple geometrical factors such as surface area and porosity are not sufficient to explain gas adsorption in MOFs.[43] We identified three different regions based on the calculated surface areas of MOFs in Figure 2c, and Figure 2d represents the similarities between the pore sizes of MOFs grouped in each region. MOFs in the same region in Figure 2c have almost the same H_2 uptakes but different CO_2 uptakes. MOFs with the highest surface areas (Cr-, Cu-, Co-, Mn-, and Fe-HKUST-1) exhibit the highest H_2 adsorption, but their CO_2 uptakes vary depending on the metal charges as shown in Table 1.

Figure 3 reveals the density plots of adsorbed CO_2 and H_2 positions in M-HKUST-1 materials for CO_2/H_2:15/85 mixture at 298 K, 10 bar. We specifically focused on three MOFs, Fe-, Cu-, and Cd-HKUST-1, since (i) Fe-HKUST-1 has the lowest CO_2 and the highest H_2 adsorption; (ii) Cu is the original metal of HKUST-1; (iii) Cd-HKUST-1 has the highest CO_2 and the lowest H_2 adsorption at 10 bar. The metal change from Fe to Cu and from Cu to Cd alters the regions that CO_2 is adsorbed in the framework due to the change in the electronic environment. As the electronic environment gets more positively charged (calculated partial charges of Fe, Cu, and

DOI: 10.1021/acs.jpcc.9b08581
J. Phys. Chem. C 2019, 123, 28255–28265

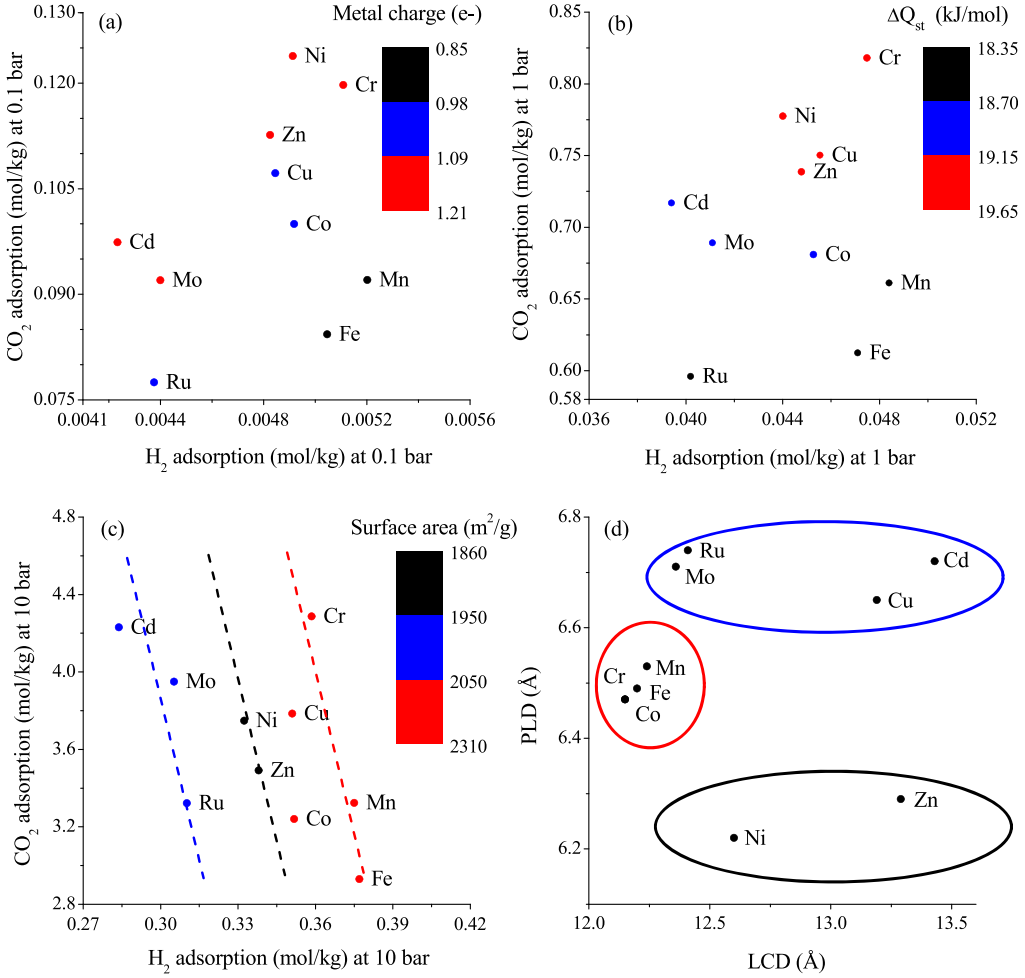


Figure 2. CO_2 and H_2 uptakes in M-HKUST-1 series at (a) 0.1, (b) 1, and (c) 10 bar and 298 K. (d) PLD and LCD of M-HKUST-1 series.

Cd are 0.85, 0.99, and 1.21 e^-, respectively) along with the decreased surface area (calculated surface areas of Fe, Cu, and Cd-HKUST-1 are 2249, 2160, and 1871 m^2/g, respectively), CO_2 tends to preferentially adsorb in the regions close to the metal sites in the large pore A in addition to the small pore B, which are shown in Figure S1a. This indicates that adsorption sites in the small pore B are the first preferential sites for CO_2 and those in the large pore A are the second ones. Figure 3a–c shows that as the effect of charge environment dominates and accessible surface area decreases as a result of metal change, the second most preferential adsorption site becomes available for the guest molecules, enhancing the CO_2 adsorption. Figure 3d–f shows that H_2 tends to be adsorbed in both small and large pores. As the partial charge of the metal increases from Figure 3d to f, adsorption of H_2 molecules is hindered due to CO_2 adsorption around the favorable adsorption sites. As a result, in contrast to being adsorbed around the most favorable adsorption sites in pore B as shown in Figure 3d, H_2 molecules are more preferentially adsorbed in pore A as shown in Figure 3e–f. Overall, these density plots of adsorbate positions provided molecular-level information about how the gas adsorption preference of M-HKUST-1 materials changes depending on the identity of metals.

Figure 4 shows CO_2 and H_2 adsorption in M-HATGUF series at pressures of 0.1, 1, and 10 bar, 298 K. Similar to Figure 2 where M-HKUST-1 was studied, metal charges, difference of heats of adsorption values between CO_2 and H_2, and surface areas of M-HATGUF materials were color-coded to examine their impacts on the adsorption of CO_2/H_2 mixture. Figure 4a shows that CO_2 adsorption generally increases with the value of metal charge at low pressure. Figure 4b shows that CO_2 adsorption increases with the values of ΔQ_{st}, whereas H_2 adsorption decreases which can be attributed to the competitive adsorption between two gases in the mixture. We also note that the values of $Q_{st}^{CO_2}$ in M-HKUST-1 were computed to vary between 23.9 and 25.5 kJ/mol whereas they were calculated to range between 24.3 and 34.0 kJ/mol for M-HATGUF series. This result indicates that changing the metal type has a more pronounced effect on the CO_2 affinity of M-HATGUF compared to M-HKUST-1. Figure 4c shows that both CO_2 and H_2 adsorptions increase with the surface area of materials whereas pore sizes shown in Figure 4d do not significantly affect the gas adsorption properties of M-HATGUF.

Figure 5 shows the density plots of adsorbed CO_2 and H_2 positions in Zn-, Cu-, and Cr-HATGUF at 10 bar, 298 K. Zn and Cr were specifically compared with Cu (the original metal of HATGUF) since the former represents the MOF having the lowest CO_2 adsorption and the latter represent the MOF having the highest CO_2 adsorption. Two specific pores were identified in M-HATGUF as pore C and D in Figure S1b. Figure 5 shows that CO_2 and H_2 are preferentially adsorbed on the same adsorption sites existing on both pore C and D. For

DOI: 10.1021/acs.jpcc.9b08581
J. Phys. Chem. C 2019, 123, 28255–28265

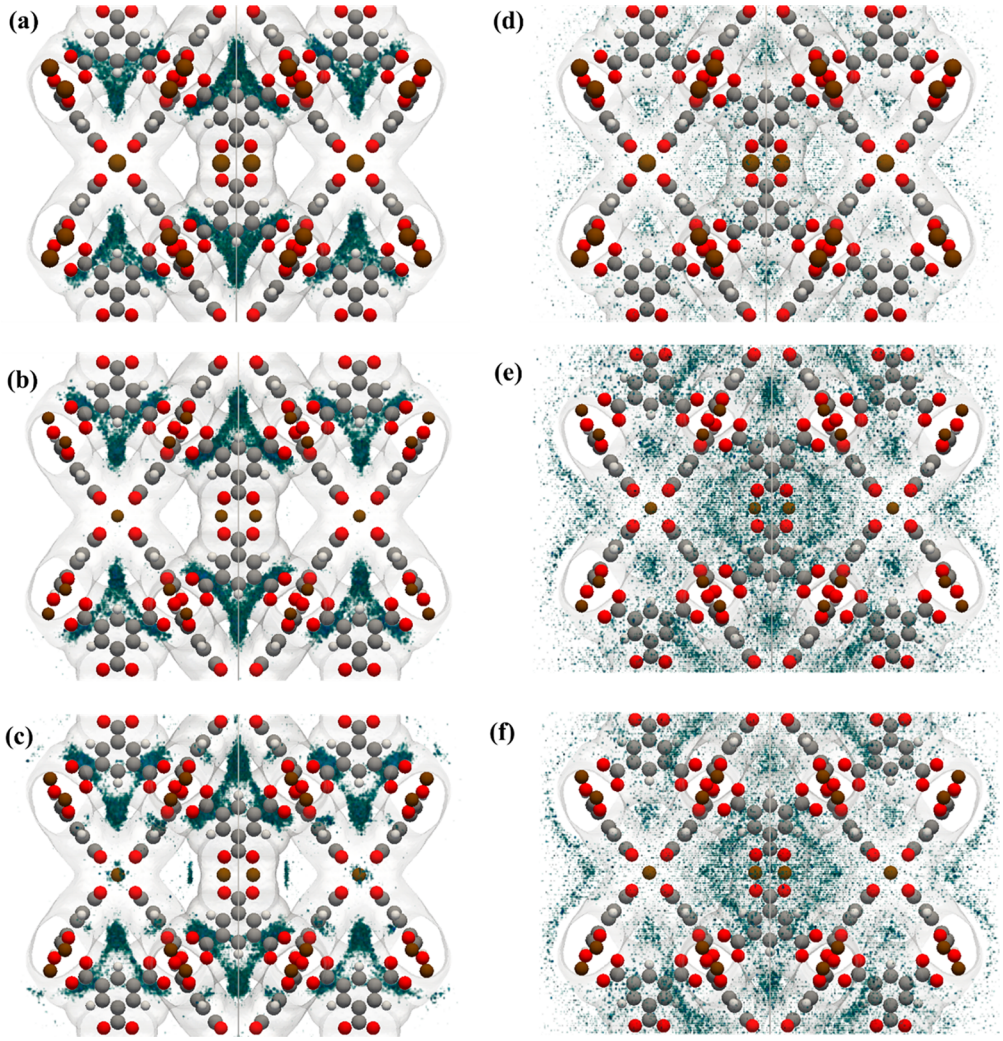


Figure 3. Density plots of adsorbed CO_2 positions within the unit cell of M-HKUST-1 where M is (a) Fe, (b) Cu, and (c) Cd at 10 bar and 298 K. Density plots of adsorbed H_2 positions within the unit cell of M-HKUST-1 where M is (d) Fe, (e) Cu, and (f) Cd at 10 bar and 298 K. Cyan dots show the locations where gas molecules were adsorbed in the GCMC simulations. Carbon, hydrogen, oxygen, and metal in the framework are represented using gray, white, red, and brown colors, respectively.

this reason and because of its lower surface area, Zn-HATGUF revealed the lowest CO_2 adsorption capacity among Zn-, Cu-, and Cr-HATGUF. CO_2 molecules preferred both pore C and D for adsorption in Zn-HATGUF (Figure 5a) while they preferred the adsorption sites available in pore C in Cu- and Cr-HATGUF as shown in Figure 5b and c, respectively. On the other hand, adsorbed H_2 molecules were more concentrated around the favorable sorption sites of Zn- and Cr-HATGUF (Figure 5d and f) leading to higher H_2 adsorption compared to Cu-HATGUF (Figure 5e).

The ultimate aim of our work is to identify the most appropriate metal types that improve CO_2/H_2 separation performances of M-HKUST-1 and M-HATGUF materials. Therefore, after evaluating CO_2/H_2 mixture adsorption in M-HKUST-1 and M-HATGUF series, we focused on how the adsorbent performance metrics of these materials change depending on the metal type of MOFs. Figure 6 shows CO_2/H_2 adsorption selectivity and CO_2 working capacity at VSA and PSA conditions for M-HKUST-1 (Figure 6a–b) and M-HATGUF (Figure 6c–d). Cu-HKUST-1 and Cu-HATGUF are the reference MOFs for the comparison of adsorbent performance metrics of M-HKUST-1 and M-HATGUF materials, and therefore their locations are marked with dotted lines in each figure. CO_2/H_2 selectivity and CO_2 working capacity of Cu-HKUST-1 were calculated as 93.34 and 0.64 mol/kg at VSA condition, and 61.11 and 3.03 mol/kg at PSA condition, respectively. Cr-HKUST-1 (selectivity of 97.64 and working capacity of 0.70 mol/kg) and Ni-HKUST-1 (100.10 and 0.65 mol/kg) outperform the original Cu-HKUST-1 at VSA condition as shown in Figure 6a. At PSA conditions, Mo-HKUST-1 (73.33 and 3.26 mol/kg), Cr-HKUST-1 (67.75 and 3.47 mol/kg), and Cd-HKUST-1 (84.43 and 3.51 mol/kg) outperform the original Cu-HKUST-1 as shown in Figure 6b. CO_2/H_2 selectivity and CO_2 working capacity of Cu-HATGUF were computed as 484.57 and 1.76 mol/kg at VSA condition, and 701.23 and 4.32 mol/kg at PSA condition, respectively. Only Cd-HATGUF (827.40 and 2.49 mol/kg) outperforms the original HATGUF at VSA condition (Figure 6c). Cd atom has the highest epsilon value and the highest metal charge among all the metals we studied for M-HATGUF series as shown in Table 1; therefore, both electrostatic and van der Waals interactions strongly favored adsorption of CO_2 over H_2, resulting in a significant selectivity improvement when Cd was used as the metal in the framework. At PSA condition

DOI: 10.1021/acs.jpcc.9b08581
J. Phys. Chem. C 2019, 123, 28255−28265

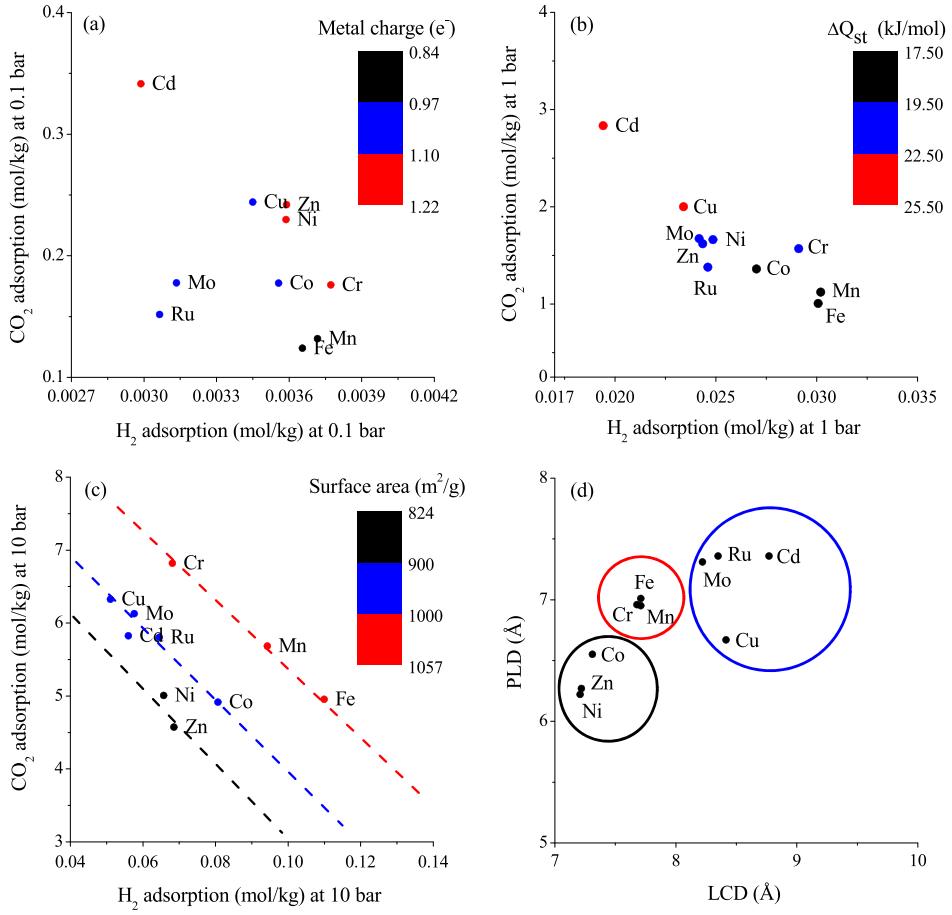


Figure 4. CO_2 and H_2 uptakes in M-HATGUF series at (a) 0.1, (b) 1, and (c) 10 bar and 298 K. (d) PLD and LCD of M-HATGUF series.

(Figure 6d), metal change in HATGUF led to improvements only in the CO_2 working capacities. Mo-HATGUF (4.46 mol/kg), Ru-HATGUF (4.42 mol/kg), Mn-HATGUF (4.56 mol/kg), and Cr-HATGUF (5.25 mol/kg) were found to have higher CO_2 working capacities than Cu-HATGUF, but none of them resulted in a selectivity enhancement.

In order to compare CO_2/H_2 selectivity and working capacity of M-HKUST-1 and M-HATGUF series, we investigated the gas−gas and gas−MOF interaction energies of MOFs in Figure S3. We showed the Coulomb and LJ energies separately. Lennard-Jones energies between adsorbates and M-HKUST-1 series were comparable with those between adsorbates and M-HATGUF series at every pressure. However, Coulomb energies between CO_2 and M-HATGUF series were greater than those between CO_2 and M-HKUST-1 series at each pressure. Higher CO_2 adsorption capacity of M-HATGUF series compared to M-HKUST-1 series can be explained by the higher CO_2−MOF Coulomb energy, and as a result of this, higher adsorption capacity, higher selectivity, and higher working capacity values were calculated for M-HATGUF series compared to M-HKUST-1 series. We so far focused on CO_2/H_2:15/85 mixture since it is close to the relevant composition for the precombustion CO_2 capture. In order to explore the effect of composition on our results, we also studied adsorption of CO_2/H_2:50/50 mixture and compared simulated CO_2 uptakes and selectivities of M-HKUST-1 and M-HATGUF with those calculated for CO_2/H_2:15/85 gas mixtures in Figure S4. At low pressures, 0.1 and 1 bar, changing the composition did not significantly affect selectivities of MOFs. At 10 bar, CO_2/H_2 adsorption selectivities were calculated to increase for M-HKUST-1 series while they were computed to slightly decrease for M-HATGUF series when the composition was changed from 15/85 to 50/50. The rankings of M-HKUST-1 and M-HATGUF series based on their CO_2 uptakes and CO_2/H_2 selectivities were found to be very similar for CO_2/H_2:15/85 and CO_2/H_2:50/50 mixtures. We computed the Spearman correlation coefficients (SRCC) which show the relationship between two independent ranking lists (one for CO_2/H_2:15/85 mixture and the other for CO_2/H_2:50/50 mixture). If the correlation between two independent rankings agrees well, SRCC reaches to 1. SRCC values for CO_2 uptakes of M-HKUST-1 and M-HATGUF series were calculated to be in the range of 0.88−0.96 and 0.75−0.99, respectively whereas SRCC values for CO_2/H_2 selectivity of M-HKUST-1 and M-HATGUF series were computed as 0.93−0.99 and 0.89−0.99, respectively, depending on the pressure.

Although selectivity and working capacity are widely used to assess the gas separation performance of MOF adsorbents, a recent approach in identifying the most promising MOFs is to rank the materials having R% > 85% based on their APS values.[9] Figure 7 shows calculated R% and APS of M-HKUST-1 (Figure 7a−b) and M-HATGUF (Figure 7c−d) at VSA and PSA conditions. We computed R% and APS of original HKUST-1 as 85.71% and 60.03 mol/kg at VSA condition, and 80.18% and 185.44 mol/kg at PSA condition. Enhancement in both metrics (R% and APS) was observed at VSA condition when the metal was changed from Cu to Cd as shown in

DOI: 10.1021/acs.jpcc.9b08581
J. Phys. Chem. C 2019, 123, 28255−28265

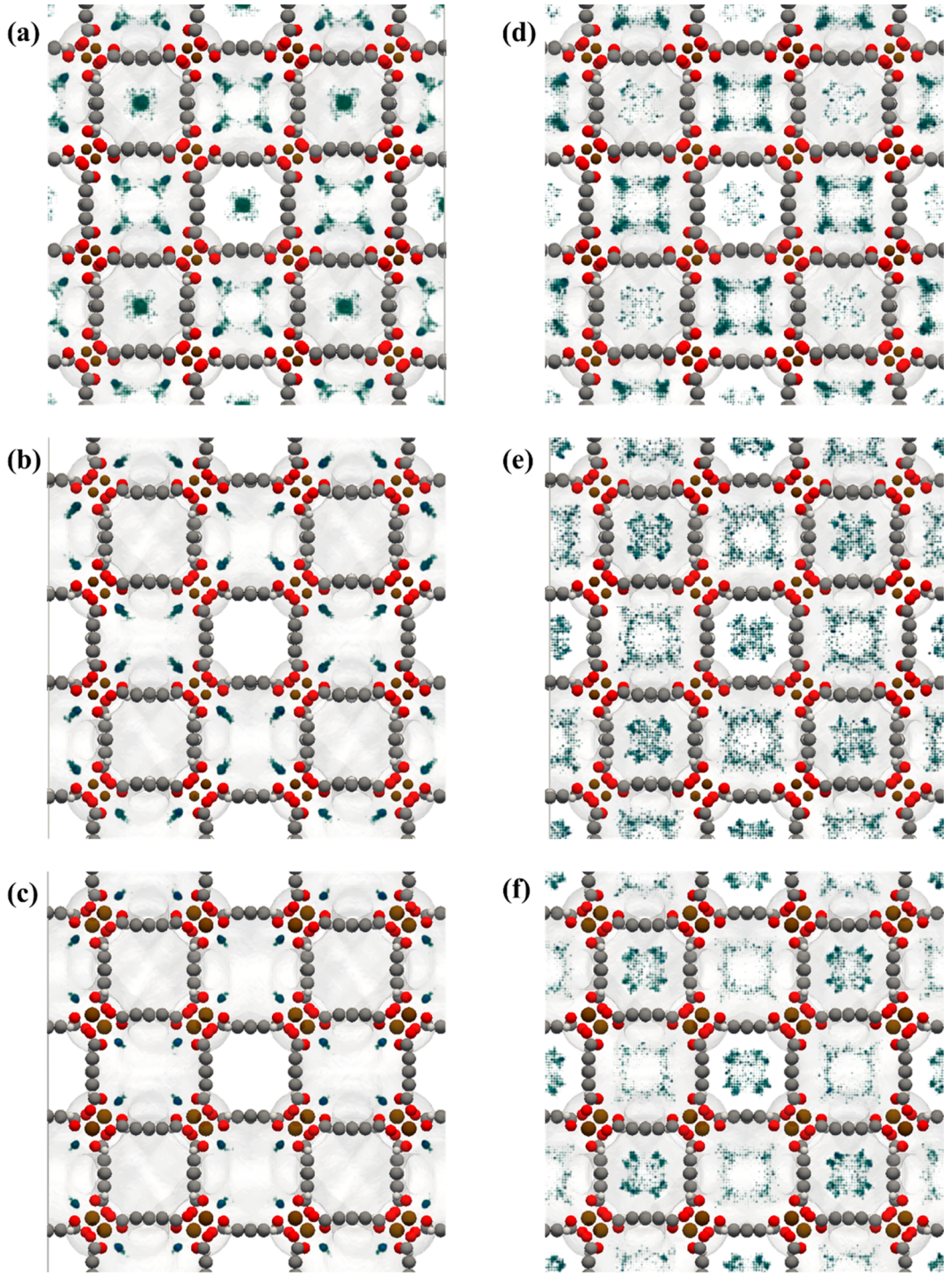


Figure 5. Density plots of adsorbed CO_2 positions within the unit cell of M-HATGUF where M is (a) Zn, (b) Cu, and (c) Cr at 10 bar and 298 K. Density plots of adsorbed H_2 positions within the unit cell of M-HATGUF where M is (d) Zn, (e) Cu, and (f) Cr at 10 bar and 298 K. Cyan dots show the locations where gas molecules were adsorbed in the GCMC simulations. Carbon, hydrogen, oxygen, and metal in the framework are represented using circles with gray, white, red, and brown colors, respectively.

Figure 7a. Cd-HKUST-1 was calculated to have R% of 86.41% and APS of 63.85 mol/kg. Figure 7b shows that improvements in both metrics were achieved when Cd, Mo, and Cr were used as metals in HKUST-1. Cd-HKUST-1 (R% of 83.05% and APS of 296.63 mol/kg), Mo-HKUST-1 (R% of 82.55% and APS of 239.11 mol/kg), and Cr-HKUST-1 (R% of 80.92% and APS of 235.01 mol/kg) outperform Cu-HKUST-1 at PSA condition. We note that APS of Cd-HKUST-1 was 1.6 times greater than that of Cu-HKUST-1, and Cd-HKUST-1 was also estimated to have the highest R% among all M-HKUST-1 materials. These results show that using Cd as the metal center in HKUST-1 leads to an adsorbent offering higher APS and R% at both VSA and PSA conditions.

R% and APS of Cu-HATGUF were computed as 87.80% and 851.35 mol/kg at VSA, and 68.36% and 3030.98 mol/kg at PSA conditions, respectively. Figure 7c shows that there is a dramatic enhancement in APS of HATGUF when Cu was changed with Cd at VSA condition. Specifically, APS of Cd-

DOI: 10.1021/acs.jpcc.9b08581
J. Phys. Chem. C 2019, 123, 28255−28265

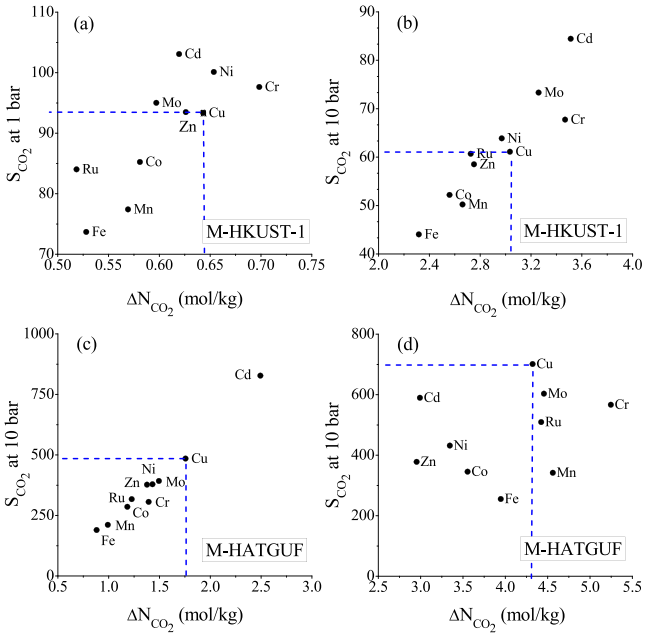


Figure 6. Calculated selectivity and working capacity for M-HKUST-1 series at (a) VSA, (b) PSA conditions. Calculated selectivity and working capacity for M-HATGUF series at (c) VSA, (d) PSA conditions.

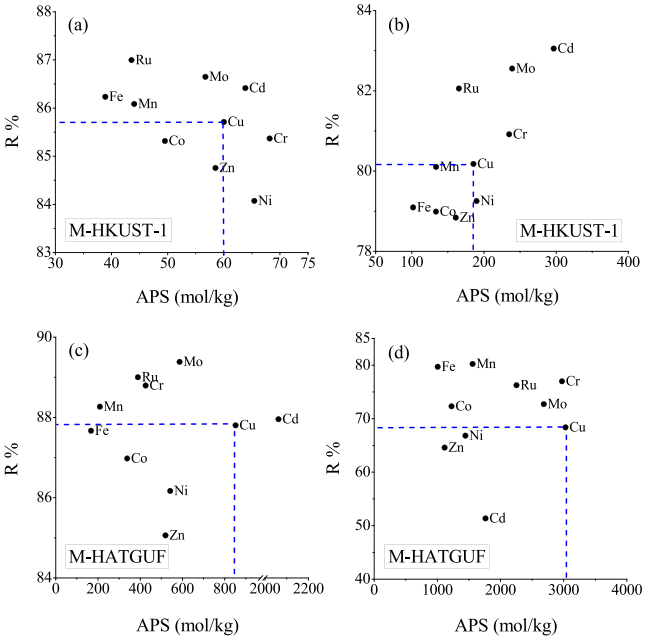


Figure 7. Calculated R% and APS for M-HKUST-1 series at (a) VSA, (b) PSA conditions. Calculated R% and APS for M-HATGUF series at (c) VSA, (d) PSA conditions.

HATGUF (2062.63 mol/kg) was more than double of Cu-HATGUF with a slightly improvement in R%. The high APS of Cd-HATGUF is due to its high CO_2/H_2 selectivity as we discussed above. The highest epsilon value and the highest metal charge value of Cd-HATGUF lead to strong interactions between CO_2 molecules and framework atoms which result in an increase in the CO_2 adsorption and a decrease in H_2 adsorption. Therefore, Cd-HATGUF revealed better separation performance than the original Cu-HATGUF that we identified to be highly promising at VSA condition in our previous computational screening study.[9] On the other hand, Figure 7d shows that using different metal sites can improve only R% without offering an enhancement in APS of HATGUF at PSA condition.

Results so far indicate the huge potential of tuning the adsorbent performance metrics of MOFs through metal change. In order to reveal the role of metal change in the adsorbent selection metrics of M-HKUST-1 and M-HATGUF, we showed the best MOFs having improvements over the original MOFs (Cu-HKUST-1 and Cu-HATGUF) in Figure 8. The first column represents the calculated value of the metrics, and the other columns represent the percentage improvements in the metric upon the metal change. For example, using Cr instead of Cu in HKUST-1 improves CO_2/H_2 selectivity, CO_2 working capacity, and APS about 5%, 9%, and 14%, respectively, without changing R% of the MOF at VSA condition. At PSA condition, using Cd or Cr significantly improves selectivity, working capacity, APS, and R% of HKUST-1. For example, Cd-HKUST-1 has 38%, 16%, 4%, and 60% enhanced CO_2/H_2 selectivity, CO_2 working capacity, R%, and APS, respectively, compared to original HKUST-1. Although there was not any MOF that exceeds the performance of Cu-HATGUF at PSA condition, excellent improvement at each metric was observed by Cd-HATGUF at VSA condition. Using Cd in HATGUF resulted in 71%, 42%, and 142% increase in selectivity, working capacity, and APS of MOF, respectively, without any change in R%. We note that computed adsorbent performance metrics of Cd-HATGUF are significantly higher than those of M-HKUST-1 series. Our results so far showed that changing metals can provide significantly promising results in terms of adsorbent performance improvements of HATGUF, but it is important to note that the stability of M-HATGUF materials should be further examined by experimental studies.

4. CONCLUSION

In this work, we investigated the influence of metal type in M-HKUST-1 and M-HATGUF materials on their CO_2/H_2 mixture separation performances using molecular simulations. We showed that upon the change of metal type, preferential CO_2 and H_2 adsorption sites of materials change, and significant improvements in several adsorbent performance metrics of M-MOF materials were achieved when Cu metal in HKUST-1 and HATGUF was changed with Cd, Co, Cr, Fe, Mn, Mo, Ni, Ru, and Zn. Cr-HKUST-1 and Cd-HKUST-1 were identified to outperform Cu-HKUST-1 in terms of selectivity and APS at both VSA and PSA conditions. For example, Cd-HKUST-1 was computed to have 38%, 16%, 4%, and 60% enhanced CO_2/H_2 selectivity, CO_2 working capacity, R%, and APS, respectively, compared to original Cu-HKUST-1 at PSA condition. Cd-HATGUF was identified to offer a significant enhancement in APS, 142% increase, compared to Cu-HATGUF, which made it a very promising MOF for a VSA process. CO_2/H_2 selectivity of HATGUF was also found to be almost doubled by changing the metal from Cu to Cd. Considering the fact that there are very large numbers of available MOFs and metals, our results revealed that CO_2/H_2 mixture separation performances of materials can be significantly improved via metal change. These results will be also useful to direct the selection of metals during the design and synthesis of new MOFs in order to achieve adsorbents having outstanding performance for CO_2 capture.

DOI: 10.1021/acs.jpcc.9b08581
J. Phys. Chem. C 2019, 123, 28255−28265

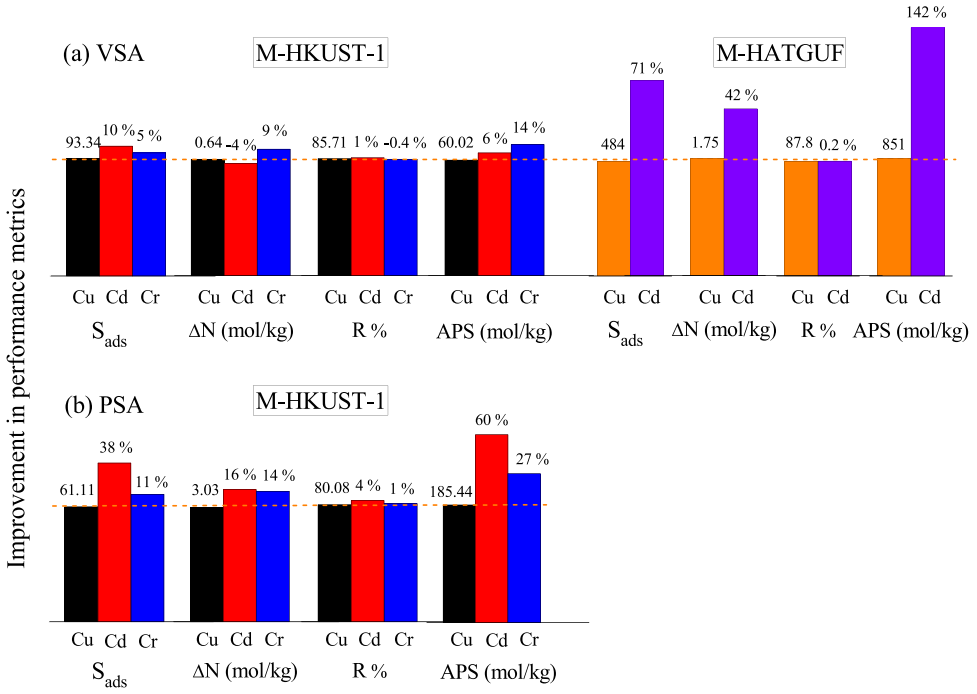


Figure 8. Percentage increase in selectivity, working capacity, R%, and APS of M-HKUST-1 and M-HATGUF. Columns in black represent calculated values of the adsorbent performance metrics for Cu-HKUST-1 and Cu-HATGUF whereas red and blue columns represent the percentage enhancement in the metrics upon the metal change.

■ ASSOCIATED CONTENT

Supporting Information

The Supporting Information is available free of charge on the ACS Publications website at DOI: 10.1021/acs.jpcc.9b08581.

Partial atomic charges for M-HKUST-1 and M-HATGUF series; adsorbent evaluation metrics used to evaluate MOF adsorbents; representation of pore structures in M-HKUST-1 and M-HATGUF; CO_2 adsorption isotherms for M-HKUST-1 and M-HATGUF at 298 K; computed interaction energies for M-HKUST-1 and M-HATGUF at 0.1, 1, and 10 bar, 298 K; CO_2 uptake and CO_2/H_2 selectivity for CO_2/H_2:50/50 and CO_2/H_2:15/85 mixtures of M-HKUST-1 and M-HATGUF at 0.1,1 and 10 bar, 298 K (PDF)

■ AUTHOR INFORMATION

Corresponding Author

*E-mail: skeskin@ku.edu.tr. Phone: +90 (212) 338-1362.

ORCID

Seda Keskin: 0000-0001-5968-0336

Notes

The authors declare no competing financial interest.

■ ACKNOWLEDGMENTS

S.K. acknowledges an ERC-2017-Starting Grant. This study has received funding from the European Research Council (ERC) under the European Union's Horizon 2020 research and innovation programme (ERC-2017-Starting Grant, grant agreement no. 756489-COSMOS).

■ REFERENCES

(1) Gangu, K. K.; Maddila, S.; Mukkamala, S. B.; Jonnalagadda, S. B. A Review on Contemporary Metal-Organic Framework Materials. *Inorg. Chim. Acta* **2016**, *446*, 61−74.

(2) Cheong, V. F.; Moh, P. Y. Recent Advancement in Metal-Organic Framework: Synthesis, Activation, Functionalisation, and Bulk Production. *Mater. Sci. Technol.* **2018**, *34*, 1025−1045.

(3) Ding, M.; Flaig, R. W.; Jiang, H.-L.; Yaghi, O. M. Carbon Capture and Conversion Using Metal-Organic Frameworks and MOF-Based Materials. *Chem. Soc. Rev.* **2019**, *48*, 2783−2828.

(4) Yuan, S.; Feng, L.; Wang, K.; Pang, J.; Bosch, M.; Lollar, C.; Sun, Y.; Qin, J.; Yang, X.; Zhang, P.; et al. Stable Metal-Organic Frameworks: Design, Synthesis, and Applications. *Adv. Mater.* **2018**, *30*, 1704303.

(5) Hu, Z.; Wang, Y.; Shah, B. B.; Zhao, D. CO_2 Capture in Metal-Organic Framework Adsorbents: An Engineering Perspective. *Adv. Sustainable Syst.* **2019**, *3*, 1800080.

(6) Altintas, C.; Avci, G.; Daglar, H.; Nemati Vesali Azar, A.; Velioglu, S.; Erucar, I.; Keskin, S. Database for CO_2 Separation Performances of MOFs Based on Computational Materials Screening. *ACS Appl. Mater. Interfaces* **2018**, *10*, 17257−17268.

(7) Daglar, H.; Keskin, S. Computational Screening of Metal-Organic Frameworks for Membrane-Based $CO_2/N_2/H_2o$ Separations: Best Materials for Flue Gas Separation. *J. Phys. Chem. C* **2018**, *122*, 17347−17357.

(8) Siegelman, R. L.; Milner, P. J.; Kim, E. J.; Weston, S. C.; Long, J. R. Challenges and Opportunities for Adsorption-Based CO_2 Capture from Natural Gas Combined Cycle Emissions. *Energy Environ. Sci.* **2019**, *12*, 2161−2173.

(9) Avci, G.; Velioglu, S.; Keskin, S. High-Throughput Screening of MOF Adsorbents and Membranes for H_2 Purification and CO_2 Capture. *ACS Appl. Mater. Interfaces* **2018**, *10*, 33693−33706.

(10) Sumer, Z.; Keskin, S. Ranking of MOF Adsorbents for CO_2 Separations: A Molecular Simulation Study. *Ind. Eng. Chem. Res.* **2016**, *55*, 10404−10419.

(11) Nandi, S.; De Luna, P.; Daff, T. D.; Rother, J.; Liu, M.; Buchanan, W.; Hawari, A. I.; Woo, T. K.; Vaidhyanathan, R. A Single-

DOI: 10.1021/acs.jpcc.9b08581
J. Phys. Chem. C 2019, 123, 28255−28265

Ligand Ultra-Microporous MOF for Precombustion CO_2 Capture and Hydrogen Purification. *Sci. Adv.* **2015**, *1*, e1500421.
(12) Chung, Y. G.; Gómez-Gualdrón, D. A.; Li, P.; Leperi, K. T.; Deria, P.; Zhang, H.; Vermeulen, N. A.; Stoddart, J. F.; You, F.; Hupp, J. T.; et al. In Silico Discovery of Metal-Organic Frameworks for Precombustion CO_2 Capture Using a Genetic Algorithm. *Sci. Adv.* **2016**, *2*, e1600909.
(13) Yaghi, O. M.; O'Keeffe, M.; Ockwig, N. W.; Chae, H. K.; Eddaoudi, M.; Kim, J. Reticular Synthesis and the Design of New Materials. *Nature* **2003**, *423*, 705−714.
(14) Cui, P.; Li, J.-J.; Dong, J.; Zhao, B. Modulating CO_2 Adsorption in Metal-Organic Frameworks Via Metal-Ion Doping. *Inorg. Chem.* **2018**, *57*, 6135−6141.
(15) Bosch, M.; Yuan, S.; Rutledge, W.; Zhou, H.-C. Stepwise Synthesis of Metal-Organic Frameworks. *Acc. Chem. Res.* **2017**, *50*, 857−865.
(16) Caskey, S. R.; Wong-Foy, A. G.; Matzger, A. J. Dramatic Tuning of Carbon Dioxide Uptake Via Metal Substitution in a Coordination Polymer with Cylindrical Pores. *J. Am. Chem. Soc.* **2008**, *130*, 10870−10871.
(17) Wu, X.; Bao, Z.; Yuan, B.; Wang, J.; Sun, Y.; Luo, H.; Deng, S. Microwave Synthesis and Characterization of MOF-74 (M = Ni, Mg) for Gas Separation. *Microporous Mesoporous Mater.* **2013**, *180*, 114−122.
(18) Waitschat, S.; et al. Synthesis of M-Uio-66 (M = Zr, Ce or Hf) Employing 2,5-Pyridinedicarboxylic Acid as a Linker: Defect Chemistry, Framework Hydrophilisation and Sorption Properties. *Dalton Trans* **2018**, *47*, 1062−1070.
(19) Wade, C. R.; Dinca, M. Investigation of the Synthesis, Activation, and Isosteric Heats of CO_2 Adsorption of the Isostructural Series of Metal-Organic Frameworks $M_3(BTC)_2$ (M = Cr, Fe, Ni, Cu, Mo, Ru). *Dalton Trans* **2012**, *41*, 7931−8.
(20) Cai, Y.; Zhang, Y.; Huang, Y.; Marder, S. R.; Walton, K. S. Impact of Alkyl-Functionalized BTC on Properties of Copper-Based Metal-Organic Frameworks. *Cryst. Growth Des.* **2012**, *12*, 3709−3713.
(21) Wu, Y.; Chen, H.; Xiao, J.; Liu, D.; Liu, Z.; Qian, Y.; Xi, H. Adsorptive Separation of Methanol-Acetone on Isostructural Series of Metal-Organic Frameworks M-BTC (M = Ti, Fe, Cu, Co, Ru, Mo): A Computational Study of Adsorption Mechanisms and Metal-Substitution Impacts. *ACS Appl. Mater. Interfaces* **2015**, *7*, 26930−40.
(22) Yu, J.; Wu, Y.; Balbuena, P. B. Response of Metal Sites toward Water Effects on Postcombustion CO_2 Capture in Metal-Organic Frameworks. *ACS Sustainable Chem. Eng.* **2016**, *4*, 2387−2394.
(23) Koh, H. S.; Rana, M. K.; Wong-Foy, A. G.; Siegel, D. J. Predicting Methane Storage in Open-Metal-Site Metal-Organic Frameworks. *J. Phys. Chem. C* **2015**, *119*, 13451−13458.
(24) Borycz, J.; Tiana, D.; Haldoupis, E.; Sung, J. C.; Farha, O. K.; Siepmann, J. I.; Gagliardi, L. CO_2 Adsorption in M-IRMOF-10 (M= Mg, Ca, Fe, Cu, Zn, Ge, Sr, Cd, Sn, Ba). *J. Phys. Chem. C* **2016**, *120*, 12819−12830.
(25) Park, J.; Kim, H.; Han, S. S.; Jung, Y. Tuning Metal-Organic Frameworks with Open-Metal Sites and Its Origin for Enhancing CO_2 Affinity by Metal Substitution. *J. Phys. Chem. Lett.* **2012**, *3*, 826−829.
(26) Canepa, P.; Arter, C. A.; Conwill, E. M.; Johnson, D. H.; Shoemaker, B. A.; Soliman, K. Z.; Thonhauser, T. High-Throughput Screening of Small-Molecule Adsorption in MOF. *J. Mater. Chem. A* **2013**, *1*, 13597−13604.
(27) Banu, A.-M.; Friedrich, D.; Brandani, S.; Düren, T. A Multiscale Study of MOFs as Adsorbents in H_2 Psa Purification. *Ind. Eng. Chem. Res.* **2013**, *52*, 9946−9957.
(28) Frost, H.; Snurr, R. Q. Design Requirements for Metal-Organic Frameworks as Hydrogen Storage Materials. *J. Phys. Chem. C* **2007**, *111*, 18794−18803.
(29) Frost, H.; Düren, T.; Snurr, R. Q. Effects of Surface Area, Free Volume, and Heat of Adsorption on Hydrogen Uptake in Metal-Organic Frameworks. *J. Phys. Chem. B* **2006**, *110*, 9565−9570.
(30) Zarabadi-Poor, P.; Marek, R. In Silico Study of (Mn, Fe, Co, Ni, Zn)-BTC Metal-Organic Frameworks for Recovering Xenon from Exhaled Anesthetic Gas. *ACS Sustainable Chem. Eng.* **2018**, *6*, 15001−15006.
(31) You, W.; Liu, Y.; Howe, J. D.; Tang, D.; Sholl, D. S. Tuning Binding Tendencies of Small Molecules in Metal-Organic Frameworks with Open Metal Sites by Metal Substitution and Linker Functionalization. *J. Phys. Chem. C* **2018**, *122*, 27486−27494.
(32) Willems, T. F.; Rycroft, C. H.; Kazi, M.; Meza, J. C.; Haranczyk, M. Algorithms and Tools for High-Throughput Geometry-Based Analysis of Crystalline Porous Materials. *Microporous Mesoporous Mater.* **2012**, *149*, 134−141.
(33) Dassault Systèmes BIOVIA, B. W. *Release 2017; BIOVIA Pipeline Pilot*, Release 2017; Dassault Systèmes, San Diego, CA.
(34) Rappe, A. K.; Casewit, C. J.; Colwell, K. S.; Goddard, W. A.; Skiff, W. M. UFF, a Full Periodic Table Force Field for Molecular Mechanics and Molecular Dynamics Simulations. *J. Am. Chem. Soc.* **1992**, *114*, 10024.
(35) Rappe, A. K.; Goddard, W. A. Charge Equilibration for Molecular-Dynamics Simulations. *J. Phys. Chem.* **1991**, *95*, 3358−3363.
(36) Wilmer, C. E.; Kim, K. C.; Snurr, R. Q. An Extended Charge Equilibration Method. *J. Phys. Chem. Lett.* **2012**, *3*, 2506−2511.
(37) Dubbeldam, D.; Calero, S.; Ellis, D. E.; Snurr, R. Q. Raspa: Molecular Simulation Software for Adsorption and Diffusion in Flexible Nanoporous Materials. *Mol. Simul.* **2016**, *42*, 81−101.
(38) Buch, V. Path Integral Simulations of Mixed Para-D_2 and Ortho-D_2 Clusters: The Orientational Effects. *J. Chem. Phys.* **1994**, *100*, 7610−7629.
(39) Potoff, J. J.; Siepmann, J. I. Vapor-Liquid Equilibria of Mixtures Containing Alkanes, Carbon Dioxide, and Nitrogen. *AIChE J.* **2001**, *47*, 1676−1682.
(40) Karavias, F.; Myers, A. L. Isosteric Heats of Multicomponent Adsorption: Thermodynamics and Computer Simulations. *Langmuir* **1991**, *7*, 3118−3126.
(41) Du, M.; Li, L.; Li, M.; Si, R. Adsorption Mechanism on Metal Organic Frameworks of Cu-BTC, Fe-BTC and ZIF-8 for CO_2 Capture Investigated by X-Ray Absorption Fine Structure. *RSC Adv.* **2016**, *6*, 62705−62716.
(42) Zhang, W.; et al. Ruthenium Metal-Organic Frameworks with Different Defect Types: Influence on Porosity, Sorption, and Catalytic Properties. *Chem. - Eur. J.* **2016**, *22*, 14297−14307.
(43) Dureckova, H.; Krykunov, M.; Aghaji, M. Z.; Woo, T. K. Robust Machine Learning Models for Predicting High CO_2 Working Capacity and CO_2/H_2 Selectivity of Gas Adsorption in Metal Organic Frameworks for Precombustion Carbon Capture. *J. Phys. Chem. C* **2019**, *123*, 4133−4139.

DOI: 10.1021/acs.jpcc.9b08581
J. Phys. Chem. C 2019, 123, 28255−28265